An Investigation of the Microstructure of a Rod/Sphere Composite Liquid

Mark A. Tracy,† Jose Luis Garcia, and R. Pecora*

Department of Chemistry, Stanford University, Stanford, California 94305-5080

Received August 28, 1992; Revised Manuscript Received December 29, 1992

ABSTRACT: Five composite liquids consisting of the rigid rod polymer poly(γ-benzyl α,L-glutamate) and narrowly dispersed, spherical silica particles were studied in the solvent dimethylformamide by dynamic (DLS) and total intensity (TILS) light scattering. The diffusion constant of the spheres was measured by DLS. The effects of sphere size, rod length, and rod concentration on the diffusion of the spheres were investigated to probe the rod solution microstructure. Microviscosities as low as one-half of the solution viscosity were determined from the sphere diffusion constants near the rod concentration c^*, which marks the onset of semidilute dynamics. At low rod concentrations, the microviscosities qualitatively follow the equation of Langevin and Rondelez,[18] indicating the solution behaves as a net rather than as a continuum. A key parameter in predicting how the spheres diffuse is the ratio of the sphere radius to the polymer mesh size (R/ξ). At higher rod concentrations, microviscosities at least 20% lower than the solution viscosity were measured for all but one composite liquid. The DLS and TILS data suggest the solution structure begins to become inhomogeneous at these higher, but prenematic, rod concentrations and that the rod solution microstructure is important in affecting sphere diffusion in this composite liquid at both low and high rod concentrations.

I. Introduction

Composite liquids are an important class of materials. For example, lubricants, paints, and adhesives are all mixtures of macromolecules in a solvent. In addition, solid composites such as polymer blends, ceramic, and controlled-release drug delivery materials are often processed in the liquid state. Thus, understanding microstructure and interactions between macromolcules in the liquid state is essential in the rational design of composites. Unfortunately, such fundamental investigations have been relatively rare due to both the difficulty of preparing precisely defined composite liquids and the lack of adequate experimental methods to monitor the motions of the various constituents.

We have recently reported the synthesis, characterization, and some studies of the dynamics of a rod/sphere composite liquid system.[1] In our case, the polymer is a rigid rod polymer, poly(γ-benzyl α,L-glutamate) (PBLG). Rigid rod polymers are frequently used in composite liquids to enhance viscosity. PBLG is commercially available in a wide range of molecular weights, and its static and dynamic behavior in dilute and nondilute solutions has been studied.[1-11] It, in addition, forms mesophases in the concentrated regime. The ceramic particles in our composite liquid are coated silica spheres. These spheres are synthesized by the method of Stöber et al.[12,13] and coated with an organic coating (3-(trimethoxysilyl)propyl methacrylate (TPM)) following a procedure based on that of Philipse et al.[1,14] to render them dispersible in organic solvents. The spheres with sizes in the range from 10 nm up to almost 1 μm can be synthesized with a relatively narrow size distribution. The solvent in our studies is dimethylformamide (DMF). Both polymer and particle are dispersible as singlets (nonaggregating) in these solvents, and the PBLG retains its rigid (or nearly rigid) rod conformation. The diffusion of both the polymer and the sphere in the composite liquid is measured by dynamic light scattering (DLS).[16] In this paper, we focus on the spheres and examine the effects of rod concentration and rod length on the diffusion of different size spheres. Total intensity light scattering (TILS) measurements were also performed on the composite liquid solutions to relate the sphere dynamics to changes in the static solution structure. This study suggests that the solution microstructure has an important influence on sphere diffusion.

* Author to whom correspondence should be addressed.
† Present address: Alkermes, Inc., 64 Sydney Street, Cambridge, MA 02139.

II. Experimental Section

Coated silica spheres of radii 39.4 and 60.4 nm (determined by DLS) were synthesized. The synthesis of the 60.4-nm particles was presented earlier.[1] The 39.4-nm particles were prepared by a similar procedure. The seed particles for the 39.4-nm spheres were synthesized from a solution of 0.18 M tetraethyl orthosilicate (TEOS), 0.6 M NH_3, and 1.53 M H_2O in absolute ethanol at 40 °C. Particles of radius 20 nm were prepared. Eight doses of TEOS were then added to the sol to grow the spheres to a radius of 40 nm. TPM (97%; 19.9 mL) was added to 212 mL of sol to coat the particles. The final coated particle radius in DMF was 39.4 nm. PBLG of molecular weights 102 000, 200 000, and 249 700 were purchased from Sigma Chemical Co. The polymer polydispersity (M_w/M_n) in each case was at most 1.2.

In the previous paper,[1] the dynamics of both binary rod/DMF and sphere/DMF solutions were studied by DLS in addition to the rod/sphere/DMF composite liquid. It was shown there that the diffusion constants of both the rods and the spheres could be simultaneously determined by DLS. It was determined that at low sphere concentrations (0.047–0.28 mg/mL (0.005–0.03 mass %)), the spheres did not alter the diffusion constants of the rods. Also, sphere/DMF solutions were studied but showed no change in the sphere diffusion constant over the dilute concentration range examined in those experiments. The dependence of the rod diffusion constants on concentration in rod/DMF solutions revealed two dynamical regimes. The transition, denoted by c^*, between these regimes was attributed to the change from dilute to semidilute dynamics. c^* was shown to be approximately equal to $1/[\eta]$.[1,15]

Results are reported here for five composite liquids (CL1–5). The constituents of each composite liquid are shown in Table I, where they are listed in order of decreasing sphere radius to rod length. Table II shows the rod concentration range for each liquid. The weight-average rod lengths, as calculated from the molecular weights, are given in Table I. The PBLG monomer molecular weight is 219 and the length per monomer is 0.15 nm. The molecular weight of the shortest rods was determined from TILS, and the manufacturer's values for the weight-average molecular weights of the other rods were used. The sphere

0024-9297/93/2226-1862$04.00/0

Table I
Composite Liquid Constituents

composite liquid	sphere radius (nm)	rod mol wt	rod length (nm)
1	60.4	102 000	70
2	60.4	200 000	137
3	60.4	249 700	171
4	39.4	200 000	137
5	39.4	249 700	171

Table II
Rod Concentrations and R/ξ Values for the Composite Liquids

rod concn (mg/mL)	nL^3	R/ξ_c	R/ξ_r	rod concn (mg/mL)	nL^3	R/ξ_c	R/ξ_r
			A. Composite Liquid 1				
1.0	2.0	1.1	0.41	15.1	30.5	2.7	5.6
3.2	6.4	1.6	1.2	20.9	42.3	3.0	7.9
5.0	10.1	1.9	1.9	29.9	60.4	3.4	11.1
10.0[a]	20.2	2.4	3.8				
			B. Composite Liquid 2				
0.20	1.6	0.51	0.078	6.0	46.4	1.5	2.3
2.0	15.5	1.1	0.78	8.5	65.8	1.6	3.3
4.0[a]	31.0	1.4	1.6	10.5	81.3	2.0	4.1
			C. Composite Liquid 3				
1.0	12.0	0.80	0.47	6.0	72.0	1.5	2.8
2.7[a]	32.5	1.1	1.3	8.4	101.3	1.6	3.9
4.0	48.0	1.3	1.9	10.1	121.8	1.8	4.8
4.6	55.4	1.4	2.2	13.1	158.0	1.9	6.2
			D. Composite Liquid 4				
0.40	3.1	0.42	0.10	5.1	39.2	0.98	1.3
0.60	4.6	0.48	0.15	6.1	47.0	1.0	1.6
0.85	6.6	0.54	0.22	7.0	54.1	1.1	1.8
3.0	23.1	0.82	0.76	8.0	61.9	1.1	2.0
3.5	26.8	0.86	0.88	10.5	81.3	1.2	2.7
4.2[a]	32.7	0.92	1.1	13.0	100.9	1.3	3.3
			E. Composite Liquid 5				
1.1	13.4	0.55	0.34	6.0	72.0	0.96	1.8
2.6[a]	31.8	0.73	0.81	8.3	100.0	1.1	2.5
4.0	48.0	0.84	1.2	10.0	120.0	1.1	3.0
4.5	54.0	0.87	1.4	13.1	158.0	1.2	4.0

[a] Rod concentration closest to but greater than c^* as determined from $[\eta]$ as described in the text.

concentrations were dilute for all five samples. A concentration of up to 0.03 mass % was used in CL1, and CL2-5 each contained 0.1% silica. The sample preparation was as previously discussed.[1] All experiments were done at 25 °C.

Each solution viscosity η was measured using three different capillary viscometers at 25 °C. Both Ostwald and Zeitfuchs cross-arm viscometers were utilized. No shear rate dependence was found. Thus, the readings from three different viscometers were averaged to determine the solution viscosity used in this paper. The error in η is the standard deviation in these readings. Using capillary viscometers, Yang[7] also did not observe shear thinning in solutions of PBLG having a length up to 190–290 nm, rods even longer than used here. Total intensity light scattering measurements were performed on the composite liquid solutions to relate the sphere dynamics to changes in the static solution structure.

DLS and TILS experiments were performed using the two apparatuses described previously.[1] The intensity autocorrelation function was measured in the homodyne DLS experiments at a minimum of three of the following angles: 25.45 or 30.56, 59.44, 90, and 110.35 or 120.56°. TILS data were taken at 30.89, 38.25, 59.47, 75.22, 97.33, 125, and 145°. Toluene was used as the reference.

For the solutions described here, the diffusion constants of the rods and the spheres were determined from the experimentally determined correlation function using the FORTRAN program CONTIN, which calculates the distribution of decay times (τ_R) leading to the decay of the measured correlation function.[1] The calculated baseline was used in all cases. The decay time (τ_R) is inversely proportional to the translational diffusion constant, D:[16]

$$\tau_R = 1/q^2D \tag{1}$$

where q is the magnitude of the scattering vector,

$$q = (4\pi n/\lambda_0)\sin(\theta/2) \tag{2}$$

and n is the solvent index of refraction, λ_0 the wavelength of the laser light in a vacuum, and θ the scattering angle. After analyzing the data with CONTIN, the sphere diffusion constants were averaged with other data taken for the same sample at the same angle. Then, $1/\tau_R$ vs q^2 plots were used to determine that the relaxation time exhibited the proper angular dependence for a diffusion process. D was independent of q over the angle range of these experiments. The final average diffusion constant presented here was determined from the slope of the linear plots. The error reported is the error in the linear least squares fit. In this paper, we focus on the effects rod and sphere size as well as rod concentration have on the diffusion constant of the spheres.

III. Dynamic Light Scattering Results and Discussion

The spheres in these composite liquid solutions are utilized as probes of the composite solution structure. In the experiments discussed here, we are interested in the question: Is the solution microstructure relevant in determining sphere diffusion? Information, although indirect, about the microscopic solution environment encountered by the spheres as they diffuse can be obtained by using the Stokes-Einstein equation to calculate the local viscosity (or microviscosity, η_μ) from the measured diffusion constants for spheres of known radius R (R is determined from DLS measurements on dilute solutions of spheres in DMF).[17]

$$\eta_\mu = kT/6\pi RD \tag{3}$$

If the microviscosity is identical to the solution viscosity (η), measured here by a capillary viscometer, the local environment encountered by the spheres appears to be the same as the average solution environment. Thus, as far as the sphere diffusion is concerned, the solution behaves as a structureless continuum—a medium completely characterized by a macroscopic property of the solution: the solution viscosity η. However, if $\eta_\mu < \eta$, the local solution environment (microstructure) surrounding the sphere as it diffuses is different from the average solution environment. This suggests that the solution microstructure is important in determining sphere diffusion.

Langevin and Rondelez[18] have presented a scaling argument to explain the case in which the probe of radius R diffuses faster through a semidilute solution of polymers than predicted from the solution viscosity. Their argument is based on topological considerations which treat the background polymer in the semidilute regime (above c^*) as a transient "net". Their argument leads to the following interpolation equation for the microviscosity:

$$\eta_0/\eta_\mu = \eta_0/\eta + \exp(-R/\xi) \tag{4}$$

where 0 signifies zero polymer concentration and ξ is the "correlation length" between polymer molecules. ξ is a measure of the mesh size of the net. The mesh size can be estimated as the average distance between the rods:

$$\xi_c = (M/cN_a)^{1/3} \tag{5}$$

It can also be estimated by the following equation:[1,30]

$$\xi_r = r_g(c^*/c) \tag{6}$$

where N_a is Avogadro's number, r_g is the radius of gyration of the polymer, and c is the polymer concentration. This equation says that at c^*, the polymers are a radius of

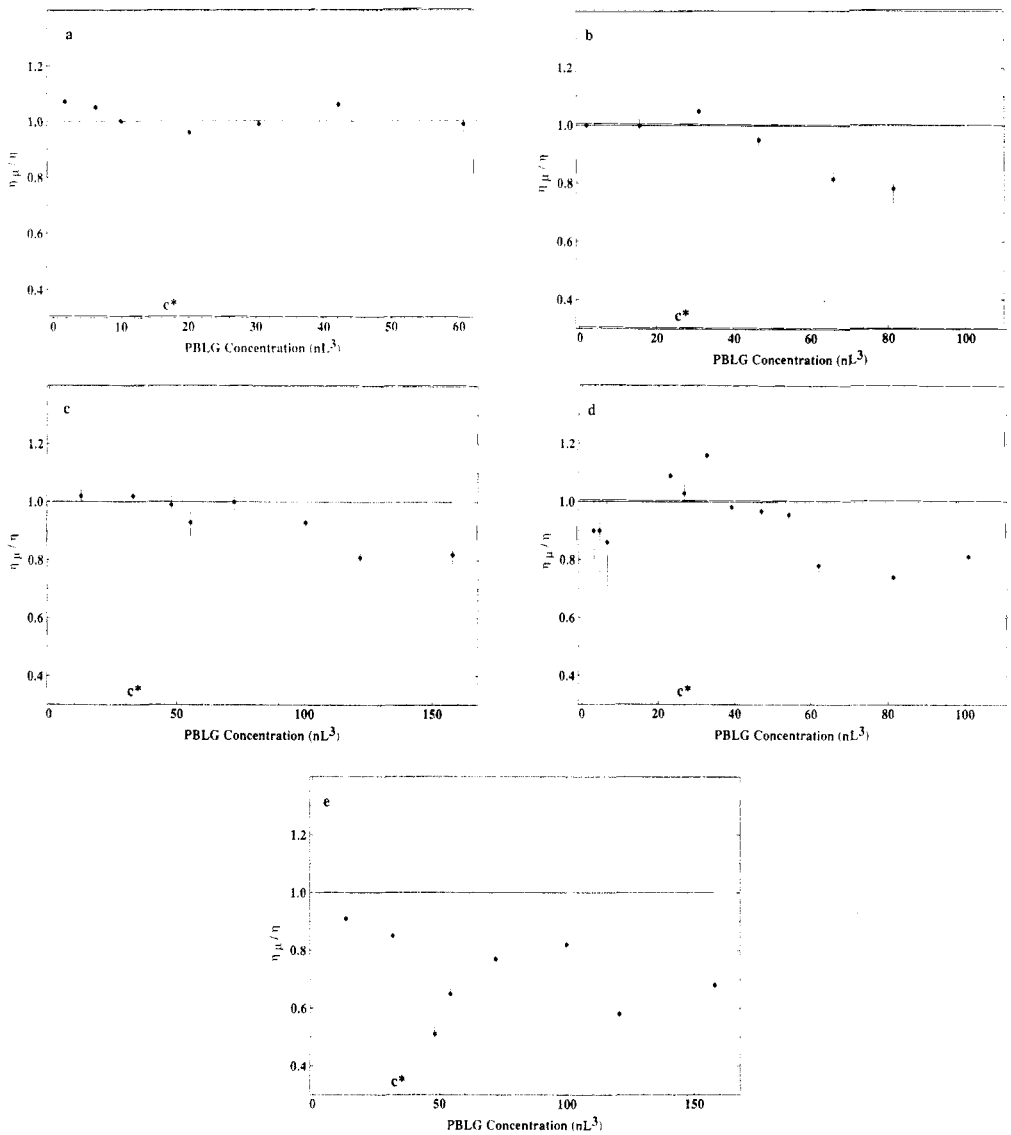

Figure 1. Microviscosity (η_μ/η) for the five composite liquids versus dimensionless rod concentration nL^3. The solid circles are the microviscosities obtained by using eq 3 to calculate η_μ from the measured D. Panel a shows the results for CL1, panel b for CL2, panel c for CL3, panel d for CL4, and panel e for CL5. They are presented in order of decreasing R/L. c^* is as described in the text.

gyration apart. The mesh size scales inversely with polymer concentration above this point. It is clear that ξ can be changed by either varying the polymer molecular weight and/or the polymer concentration.

According to eq 4, if $R \gg \xi$, $\eta_\mu \approx \eta$. But, as the probe size becomes less than the net hole size, the probes are able to diffuse through the holes and, thus, encounter a local viscosity that approaches that of the solvent, DMF. As the rod concentration increases, the mesh size decreases so η_μ again approaches η. The situation where $\eta_\mu \gg \eta$ is often indicative of aggregation or polymer adsorption onto the spheres.[17,19-22] There is no indication of aggregation or polymer adsorption in our case.

These ideas were tested by systematically varying the sphere size, rod length, and rod concentration. (η_μ/η was found to be independent of sphere concentration as is discussed below.) The results for CL1–5 are shown in Figure 1. The microviscosities were calculated from the sphere diffusion constants measured by DLS using eq 3. The errors shown in Figure 1 were calculated by a standard propagation of errors in the sphere diffusion constant and the solution viscosity.

The composite liquids in Figure 1 are presented in order of decreasing R/L. Table II shows the range of values for R/ξ determined using both eqs 5 and 6. According to Langevin et al.,[18] a mesh is only physically meaningful above c^*. Figure 1a shows that $\eta_\mu \approx \eta$ at all concentrations for CL1. Figures 1b–d show that at the low rod concentrations, $\eta_\mu \approx \eta$. The large errors in the three points at the lowest concentrations in Figure 1d are due to the fact that the inverse Laplace transform program CONTIN had difficulty resolving the sphere and rod diffusion peaks because their relaxation times were so similar. For CL5, η_μ was as small as one-half of η at the low concentrations. The only difference between CL3 and CL5 is the sphere size. The main distinction between CL4 and CL5 is the rod molecular weight. It is important to note that viscosities of solutions of 60.4-nm silica spheres in DMF (no rods) were found to increase only 2.4% as the sphere concentration increased from 0 to 0.5 mass %. Near the concentration c^* marking the onset of semidilute dynamics, the deviation from $\eta_\mu/\eta = 1$ is largest in Figure 1e, and then η_μ approaches η. This is qualitatively in accordance with eq 4, where the ratio R/ξ must be sufficiently small in order to measure $\eta_\mu < \eta$. This qualitative agreement with eq 4 suggests that above c^* the rod solution can be treated as a net as far as the diffusion of the spheres is concerned. The sphere is sufficiently small so that it diffuses through holes in the net. Adding more polymer decreases the hole size. Thus, gaps in the net become too small to be probed by the spheres, and η_μ again approaches η. These results suggest that R/ξ is an important parameter

affecting the diffusion of the spheres in these liquids, especially near c^*.

Microviscosities this much (≫10%) smaller than the solution viscosity have not previously been reported for nonaqueous solutions of spheres and coil or rod polymers, including those containing silica spheres.[23-25] In these other experiments, the background polymer was either polyisobutylene[23,25] or poly(methyl methacrylate)[24] in a nonaqueous solvent. In these studies, $3.3 < R/\xi < 45.6$, where ξ was determined from the polymer translational diffusion constant using the Stokes–Einstein equation: $\xi = kT/6\pi\eta_0 D$. Thus, it is possible in these silica sphere/coil polymer solutions that R/ξ was too large at all concentrations studied above the polymer overlap point to measure results similar to ours.

Behavior where $\eta_\mu/\eta \ll 1$ has, however, been observed before by other investigators studying aqueous solutions of polystyrene spheres in a variety of polymers.[17,22,26-32] The results of these studies do not follow the predictions of Langevin et al.[18] For example, Phillies[31] found that increasing the polymer concentration or the probe radius (up to 1–3 μm) usually resulted in a larger difference between the microviscosity and the solution viscosity. He also reported microviscosities up to a factor of 8 times smaller than the solution viscosity at large polymer molecular weights in some aqueous polystyrene sphere/polymer systems.[32] In a study of polystyrene spheres in (hydroxypropyl)cellulose, Yang and Jamieson[30] observed η_μ/η to decrease with increasing polymer concentration. They also found these deviations to increase with decreasing probe size and increasing molecular weight.

Like Phillies[31] and Yang et al.,[30] we found deviations from $\eta_\mu/\eta = 1$ at the highest polymer concentrations for all composite liquids but CL1. As shown in Figure 1, the microviscosities are about 20–30% lower than η in each case. It is also interesting to note that the higher concentration deviations begin at about 8 mg/mL PBLG regardless of the sphere size or rod molecular weight (compare Table II and Figures 1b–e). This point will be discussed in more detail in the next section.

Although no satisfactory theory exists to explain the results at the higher concentrations, $\eta_\mu \ll \eta$ has now been observed in nonaqueous solutions of rodlike polymers in addition to aqueous solutions of semiflexible and coil polymers. Possible explanations include coupling between the rod and sphere motions at the higher concentrations.[23-24] Cantor[33] found η_μ to be up to 35% less than η for polystyrene coil probes in a poly(*n*-hexyl isocyanate) rod polymer solution. Since the deviations were greatest at the highest concentrations, Cantor suggested that cooperative motions between the coils and the rods may perturb the diffusion of the probe, resulting in $\eta_\mu < \eta$.

An alternative view is that the behavior at high rod concentrations is due to a transition in the solution structure brought on by the complex interactions between the composite solution components. The idea here is that the transitions discussed below create inhomogeneities in the microstructure that could result in spheres diffusing through local environments that are different from the average solution environment. These inhomogeneities may arise mainly from sphere–rod interactions which are responsible for polymer-induced phase separation in colloidal suspensions.[34-37] Or they may be due primarily to rod–rod interactions, which have been found to cause both a prenematic transition in PBLG/DMF solutions[3] and inhomogeneities in pulp fiber suspensions.[38] These phenomena are discussed as possible explanations for our data in the following.

It has been proposed by Gast et al.[34-36] that phase separation into colloid-rich and colloid-poor phases stems from an attraction between the particles that results from purely repulsive interactions between the colloid particles and the neighboring polymer molecules. The depletion of polymer in the region between two neighboring particles creates a region of lower osmotic pressure compared to the bulk solution, resulting in a net attraction between the particles.[34] A schematic of the phase diagram for a hard sphere/coil polymer system is shown in Figure 2. No equivalent diagram was calculated for sphere/rod systems. At high volume fractions of particles a fluid–solid transition occurs at all polymer concentrations. This is the colloidal sphere order–disorder transition that occurs for hard spheres at a volume fraction (ϕ_s) of 0.497. At this point, the ordered (solid) phase has $\phi_s = 0.551$. Composite liquids 1–5 are very far from this phase boundary. Gast et al.[34] note that as the polymer and particle sizes become comparable ($R/r_g \to 1$), a fluid–fluid transition emerges as shown in Figure 2 (the curved phase boundary). This boundary is present in soft sphere/coil systems as well.[34,36] As the boundary is crossed from the region labeled Fluid A to the Fluids B region, a homogeneous polymer/sphere solution separates into two liquid phases differing in the sphere concentration. As R/r_g increases, the transition moves to lower polymer concentration. For the composite liquids containing the 60.4-nm radius spheres $1.2 < R/r_g < 3.0$ and for those with the 39.4-nm spheres $0.8 < R/r_g < 1.0$. This transition has been found to occur at very low sphere and polymer concentrations—well within the concentration ranges of the five composite liquids studied here.[34,39] A clear solution turning cloudy is usually indicative of such a transition.[39] This was not observed in our samples. However, the final post-transition solution microstructure is very likely dependent on how far the solution is initially from the phase boundary just as with polymer blends.

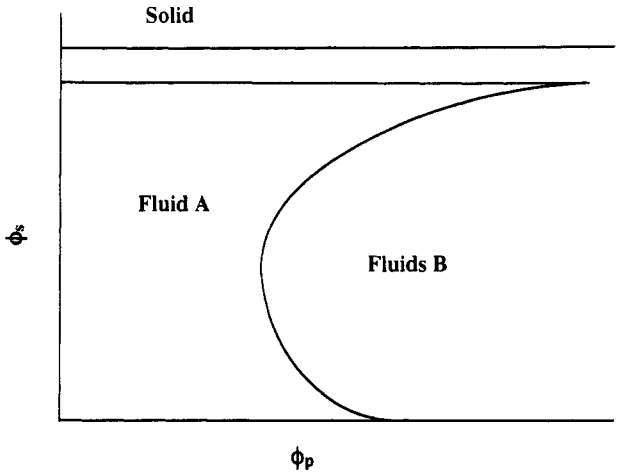

Figure 2. Schematic phase diagram for colloid–polymer solutions. ϕ_p is the polymer volume fraction in the solution. ϕ_s is the colloidal sphere volume fraction. The curved phase boundary is a fluid–fluid boundary. Fluid A is a single-phase polymer/sphere solution. Fluids B consist of two fluid phases that differ in sphere concentration. The horizontal line intersecting the fluid–fluid boundary marks the sphere order–disorder transition. For hard spheres this occurs at $\phi_s = 0.497$. This figure is based on the theory of Gast, Russel, and Hall.[34]

Experiments were performed to investigate the dependence of the measured microviscosity on the sphere concentration. Composite liquids 3 and 5 were selected for this study because they had the largest deviations from $\eta_\mu/\eta = 1$ (Figure 1). Two rod concentrations from CL5, 4.0 and 10.0 mg/mL, and one from CL3, 10.1 mg/mL, were examined. For each of the three rod concentrations, the sphere concentration was varied as shown in Table III. The number of spheres in a 0.03% solution of 39.4-nm silica is equal to the number in a 0.1% dispersion of 60.4-

Table III
Sphere Concentration Study Results

composite liquid	rod concn (mg/mL)	sphere concn (mass %)	sphere concn (mg/mL)	η_μ/η
5	4.0	0.03	0.28	0.62
5	4.0	0.06	0.56	0.54
5	4.0	0.1	0.94	0.51
5	10.0	0.03	0.28	0.59
5	10.0	0.06	0.56	0.63
5	10.0	0.1	0.94	0.58
3	10.1	0.03	0.28	0.80
3	10.1	0.06	0.56	0.80
3	10.1	0.1	0.94	0.81

nm silica. Table III reveals that there is no significant dependence of η_μ/η on the sphere concentration. This was previously shown to be the case for CL1.[1] It is possible the sphere concentration was not low enough here to cross the fluid–fluid phase boundary (Figure 2).

More compelling evidence for a change in the silica sphere/PBLG/DMF solution structure at the higher polymer concentrations comes from the results of Kerekes et al.[38] and from TILS experiments described in detail in the next section. At high rod concentrations, rods are known to form ordered (liquid crystalline) regions.[11] Kerekes et al.[38] photographed aqueous solutions of macroscopic pulp fibers at increasing rod concentrations, but below concentrations in which ordering occurs. These fibers were dispersed before the photographs were taken by mixing the solution with a vertical plunger. Their photographs show a uniform distribution of rods in the solution at low concentrations, but as the concentration increases (if $L/d > 50$) solution nonuniformity increases. For our PBLG rods, L/d = 34, 66, and 82 for molecular weights 102 000, 200 000, and 249 700, respectively. They observe flocs appearing in their solutions as the concentration increases in the regime $2 < nL^3 < 120$. (In our studies, $nL^3 \leq 158$ as shown in Table II.) The flocs in this concentration range were characterized as "loose", "unconnected", and "easily dispersed by hydrodynamic forces". Those forming at higher rod concentrations were "difficult to disperse". Our DLS results do not show evidence for a slow mode that may arise if there were PBLG flocs in solution. Perhaps in our solutions the flocs were so easily dispersed by thermal fluctuations in the solution that they did not persist for a long enough time to be detected by DLS. DeLong et al.,[3] however, observed up to four modes for PBLG (M = 277 000) in DMF including a very slow mode at concentrations higher than studied here. This mode is resolved from faster modes beginning at a concentration of about 20 mg/mL. Slow modes have also been observed in nondilute, aqueous solutions of rodlike DNA and remain unexplained.[40-46] The results of Kerekes et al.[38] offer evidence that rod solution microstructure begins to become less uniform as the concentration increases in the range covered by our experiments even without spheres. At the very least, the spheres serve to probe these changes as reflected in the DLS results. In addition, they may play a further role, perhaps even in promoting these solution inhomogeneities, suggested by TILS results presented in the next section.

IV. Total Intensity Light Scattering Results and Discussion

To investigate the static solution microstructure in more detail, TILS experiments were completed on the composite liquids. Data were taken for CL3 and CL4 using the same samples used in the DLS studies. All the data for each composite liquid were taken at a constant laser power.

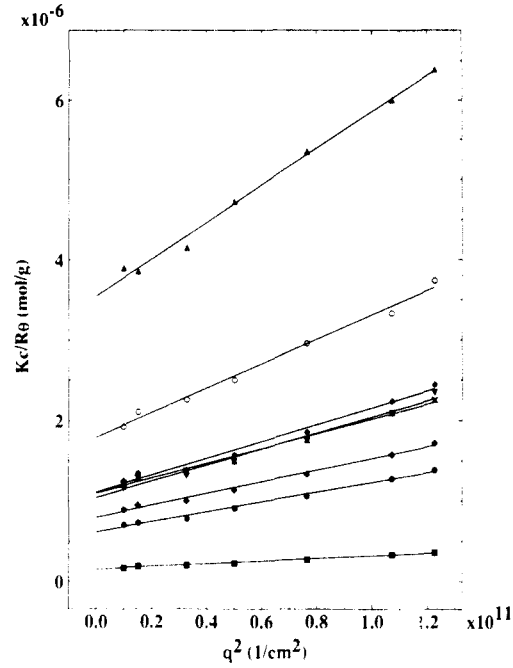

Figure 3. TILS data for CL3 at different rod concentrations. The lines are least squares linear fits to the data. (■) 1.0, (●) 2.7, (+) 3.98, (×) 4.61, (▲) 6.02, (♦) 8.36, (▼) 10.11, and (○) 13.12 mg/mL 249 700 g/mol rods.

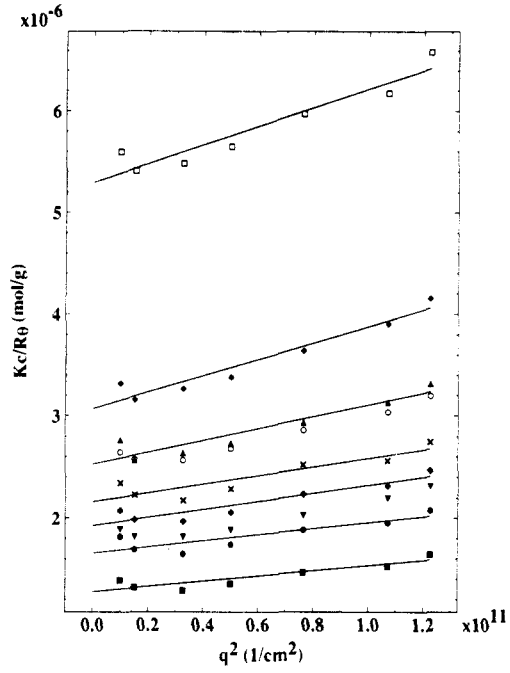

Figure 4. TILS data for CL4 at different rod concentrations. The lines are least squares linear fits to the data. (■) 2.98, (●) 3.46, (+) 4.25, (×) 5.06, (▲) 6.0, (♦) 6.98, (▼) 8.0, (○) 10.5, (□) 13.0 mg/mL 200 000 g/mol rods.

Kc/R_θ was plotted against q^2 for each rod concentration c (Figures 3 and 4). The sphere concentration is constant in each case. To eliminate any form factor effects, the intercepts from these plots were determined according to eq 7:[3]

$$Kc/R_\theta = (1/RT)(d\pi/dc)_{T,P}(1 + \xi^2 q^2) \qquad (7)$$

Here $K = 4\pi^2 n^2 (dn/dc)^2/\lambda_0^4 N_a$, where dn/dc is the specific refractive index increment. R_θ is the Rayleigh ratio and is proportional to the measured scattered light intensity. R is the gas constant, $d\pi/dc$ is an effective osmotic modulus at constant temperature and pressure, and ξ the correlation length. The osmotic modulus represents the resistance of

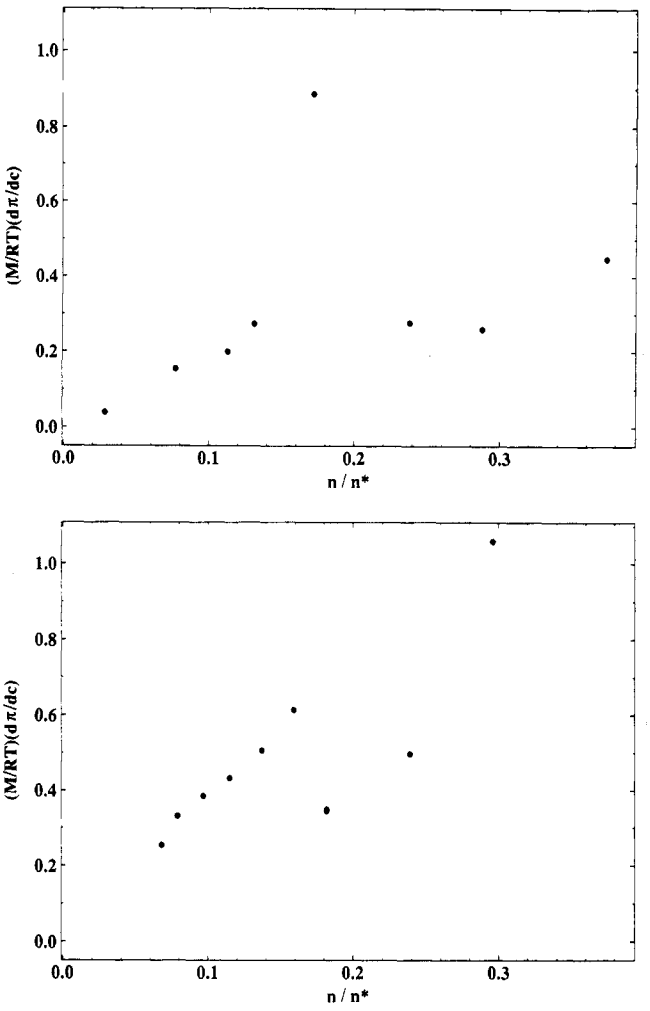

Figure 5. Variation in the scattered light intensity with rod concentration at constant sphere concentration (0.1%). The rod molecular weight times the intercepts from Figure 3 (top) (CL3) and Figure 4 (bottom) (CL4) are plotted versus rod concentration normalized by n^* (see text). Both data sets show a large change in the scattered light intensity around $n/n^* = 0.18$.

a solution to fluctuations in concentration.[3] The intercepts from Figures 3 and 4 were multiplied by the rod molecular weight and plotted against the rod concentration in Figure 5. The rod number concentration n is normalized by $n^* = 16/\pi dL^2$, a theoretical nematic transition point that is not the same as c^*. The data were plotted this way so as to be easily compared to the TILS results of DeLong and Russo[3] (their Figure 1) for concentrated solutions of PBLG without spheres in DMF. Figure 5 shows a dramatic variation in the scattered light intensity near $n/n^* \approx 0.18$ or 8 mg/mL PBLG ($nL^3 = 101.3$ for CL3 and 61.9 for CL4) for both molecular weights. This point corresponds closely to the point where the high-concentration deviations from $\eta_\mu/\eta = 1$ begin in Figures 1c,d for the same samples.

TILS experiments were also performed on the samples in Table III, and the value $(M/RT)(d\pi/dc)$ was plotted against the sphere concentration as shown in Figure 6. This plot shows that, at constant rod concentration, small variations in the sphere concentration (for example due to indeterminate variations during sample preparation) do not lead to the scattered intensity variations seen in Figure 5 near 8 mg/mL rods. A plot of Kc_{sphere}/R_θ versus the sphere concentration is given in Figure 7. Here, K is as in Figures 3 and 4. The positive slopes of these lines suggest a positive value for the thermodynamic second virial coefficient A_2 for the spheres. More data are needed to obtain a precise value for A_2.

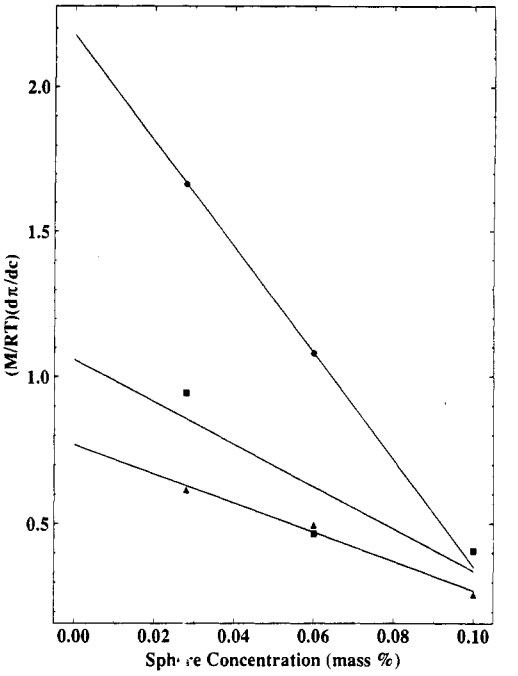

Figure 6. Variation in the scattered light intensity with sphere concentration at a constant rod concentration. (■) CL5, 4.0 mg/mL rods; (●) CL5, 10.0 mg/mL rods; (▲) CL3, 10.1 mg/mL rods.

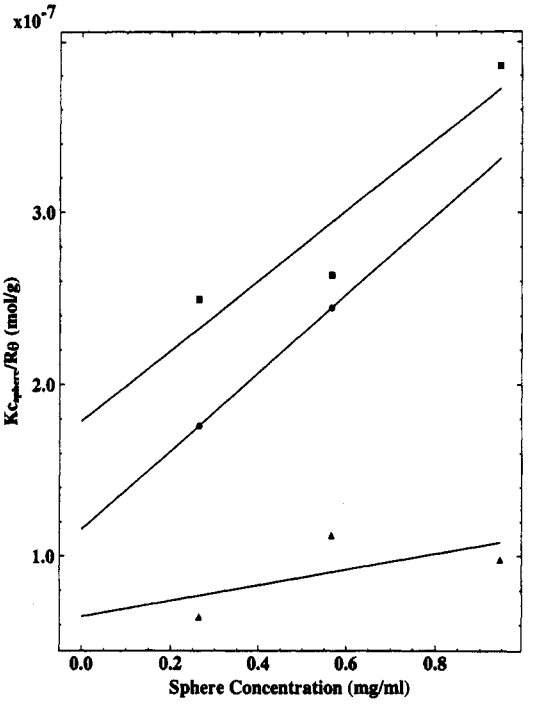

Figure 7. Kc_{sphere}/R_θ versus sphere concentration. (■) CL5, 4.0 mg/mL rods; (●) CL5, 10.0 mg/mL rods; (▲) CL3, 10.1 mg/mL rods. The lines are linear least squares fits to the data. The slopes of the lines are 2.05×10^{-4}, 2.29×10^{-4}, and 4.56×10^{-5} cm^3 mol/g^2, respectively.

DeLong and Russo[3] report an increase followed by a decrease in the osmotic modulus (y axis of Figure 5) at $n/n^* \approx 1.5$ for PBLG of $M = 277\,000$. They attribute this to the coupling of orientation and concentration fluctuations as the nematic transition is approached. This transition does not appear to be precisely correlated with the appearance of the slowest mode in their DLS results. DeLong and Russo[3] found that the slow mode became prominent at $n/n^* \approx 0.7$, whereas the transition occurred at $n/n^* \approx 1.5$. They further point out that this prenematic transition is evident at concentrations lower than required

for the formation of an equilibrium nematic phase. This occurs at ≈17.5 mass % ($n/n^* \approx 4$) for PBLG of their molecular weight. Also, when examined under crossed polarizers, even their most concentrated sample did not show any sign of an ordered phase. Thus, they observed evidence for structural change in the rod solution even before nematic phase separation occurs. This may be related to the nonuniformities observed by Kerekes et al.[38]

In Figure 5, a similar increase and decrease in the osmotic modulus is observed at $n/n^* \approx 0.18$ for both molecular weights. The upturn at the highest rod concentration is likely a reflection of rod crowding which inhibits concentration fluctuations and thus reduces the scattered light intensity. The qualitative similarity of Figure 5 to the results of DeLong and Russo[3] (their Figure 1) suggests that the peak in Figure 5 may be the same transition they observe but shifted to lower rod concentrations because of the presence of the spheres. The results of DeLong and Russo[3] combined with those here suggest the rod solution structure undergoes significant change even before the nematic phase transition. The spheres appear to trigger these changes at even lower rod concentrations. Finally, though it seems unlikely that polymer-induced phase separation is being observed in our samples, the solution structure changes below the nematic transition point suggested by DeLong and Russo[3] and the results of Kerekes et al.[38] offer a possible explanation for our TILS and DLS results at the highest rod concentrations studied.

V. Conclusion

We have performed DLS and TILS experiments on a new composite liquid containing rod and spherical macromolecules in the solvent DMF. DLS measurements indicate that the local viscosity (η_μ) encountered by the spheres was as small as one-half of the solution viscosity (η). To our knowledge, $\eta_\mu \ll \eta$ has not been previously observed for sphere diffusion in nonaqueous solutions of rigid rod polymers; however, it has been seen in aqueous solutions of coil or semiflexible polymers.[17,22,26-32] Our data suggest that the picture of Langevin et al.[18] in which the polymer solution is viewed as a "net" with holes rather than as a continuum qualitatively explains the microviscosity behavior around c^*. Currently though, there are no theories or computer simulations that predict the results at all polymer concentrations. The combination of DLS and TILS indicates that $\eta_\mu \ll \eta$ and enhanced scattering at higher rod concentrations may reflect the onset of changes in the rod solution microstructure even before the nematic transition. Recent experimental evidence[3,38] for microstructural changes in solutions of rods in a solvent supports this idea. Clearly, more experiments on well-defined composite liquids like this one are needed to fully understand the complex dynamics and microstructure in these solutions.

Acknowledgment. This work was supported by National Science Foundation Grant CHE-9119676 to R.P. and by the NSF-MRL program through the Center for Materials Research at Stanford University.

References and Notes

(1) Tracy, M. A.; Pecora, R. *Macromolecules* **1992**, *25*, 337.
(2) Russo, P. S.; Karasz, F. E.; Langley, K. H. *J. Chem. Phys.* **1984**, *80*, 5312.
(3) DeLong, L. M.; Russo, P. S. *Macromolecules* **1991**, *24*, 6139.
(4) Zero, K. M.; Pecora, R. *Macromolecules* **1982**, *15*, 87.
(5) Itou, S.; Nishioka, N.; Norisuye, T.; Teramoto, A. *Macromolecules* **1981**, *14*, 904.
(6) Matheson, R. R., Jr. *Macromolecules* **1980**, *13*, 643.
(7) Yang, J. T. *J. Am. Chem. Soc.* **1959**, *81*, 3902.
(8) Schmidt, M. *Macromolecules* **1984**, *17*, 553.
(9) Kubota, K.; Chu, B. *Biopolymers* **1983**, *22*, 1461.
(10) Kubota, K.; Tominaga, Y.; Fujime, S. *Macromolecules* **1986**, *19*, 1604.
(11) Tracy, M. A.; Pecora, R. *Annu. Rev. Phys. Chem.* **1992**, *43*, 525.
(12) Stöber, W.; Fink, A.; Bohn, E. *J. Colloid Interface Sci.* **1968**, *26*, 62.
(13) Bogush, G. H.; Tracy, M. A.; Zukoski, C. F., IV *J. Non-Cryst. Solids* **1988**, *104*, 95.
(14) Philipse, A.; Vrij, A. *J. Colloid Interface Sci.* **1989**, *128*, 121.
(15) Brown, W.; Mortensen, K. *Macromolecules* **1988**, *21*, 420.
(16) Berne, B. J.; Pecora, R. *Dynamic Light Scattering*; John Wiley and Sons: New York, 1976.
(17) Mustafa, M.; Russo, P. S. *J. Colloid Interface Sci.* **1989**, *129*, 240.
(18) Langevin, D.; Rondelez, F. *Polymer* **1978**, *19*, 875.
(19) Nehme, O. A.; Johnson, P.; Donald, A. M. *Macromolecules* **1989**, *22*, 4326.
(20) Russo, P. S.; Mustafa, M.; Cao, T.; Stephens, L. K. *J. Colloid Interface Sci.* **1988**, *122*, 120.
(21) Brown, W.; Rymdén, R. *Macromolecules* **1986**, *19*, 2942.
(22) Brown, W.; Rymdén, R. *Macromolecules* **1987**, *20*, 2867.
(23) Zhou, P.; Brown, W. *Macromolecules* **1989**, *22*, 890.
(24) Brown, W.; Rymdén R. *Macromolecules* **1988**, *21*, 840.
(25) Brown, W.; Zhou, P. *Macromolecules* **1989**, *22*, 4031.
(26) Jamieson, A. M.; Southwick, J. G.; Blackwell, J. *J. Polym. Sci., Polym. Phys. Ed.* **1982**, *20*, 1513.
(27) Turner, D. N.; Hallett, F. R. *Biochim. Biophys. Acta* **1976**, *451*, 305.
(28) Laurent, T. C.; Persson, H. *Biochim. Biophys. Acta* **1963**, *78*, 351.
(29) Phillies, G. D. J.; Ullmann, G. S.; Ullmann, K.; Lin, T.-H. *J. Chem. Phys.* **1985**, *82*, 5242.
(30) Yang, T.; Jamieson, A. M. *J. Colloid Interface Sci.* **1988**, *126*, 220.
(31) Phillies, G. D. J. *J. Phys. Chem.* **1989**, *93*, 5029.
(32) Phillies, G. D. J.; Malone, C.; Ullmann, K.; Ullmann, G. S.; Rollings, J.; Yu, L.-P. *Macromolecules* **1987**, *20*, 2280.
(33) Cantor, A. Ph.D. Thesis, Stanford University, 1991.
(34) Gast, A. P.; Russel, W. B.; Hall, C. K. *J. Colloid Interface Sci.* **1986**, *109*, 161.
(35) Gast, A. P.; Hall, C. K.; Russel, W. B. *J. Colloid Interface Sci.* **1983**, *96*, 251.
(36) Gast, A. P.; Hall, C. K.; Russel, W. B. *Faraday Discuss. Chem. Soc.* **1983**, *76*, 189.
(37) Sperry, P. R. *J. Colloid Interface Sci.* **1984**, *99*, 97.
(38) Kerekes, R. J.; Schell, C. J. *J. Pulp Pap. Sci.* **1992**, *18*, 32.
(39) Marr, D.; personal communication.
(40) Goinga, H. T.; Pecora, R. *Macromolecules* **1991**, *24*, 6128.
(41) Lin, S.; Lee, W.; Schurr, J. M. *Biopolymers* **1978**, *17*, 1041.
(42) Schmitz, K. S.; Lu, M.; Singh, N.; Ramsay, D. J. *Biopolymers* **1984**, *23*, 1637.
(43) Fried, M. G.; Bloomfield, V. A. *Biopolymers* **1984**, *23*, 2141.
(44) Nicolai, T.; Mandel, M. *Macromolecules* **1989**, *22*, 438.
(45) Nicolai, T.; Mandel, M. *Macromolecules* **1989**, *22*, 2348.
(46) Wang, L.; Garner, M. M.; Yu, H. *Macromolecules* **1991**, *24*, 2368.